Advances in the Prevention of Investment Casting Defects Assisted by Computer Simulation

Jörg Fischer-Bühner
Dr.-Ing.
The Research Institute for Precious Metals (FEM)
Schwäbisch Gmünd, Germany

Abstract

Computer simulation of investment casting has recently been identified as a powerful tool for giving new insight into defect generation mechanisms, especially those related to form filling, shrinkage porosity and gas porosity caused by reaction with investment material.[1–3] While previous work of the author's group mainly focused on simulation of silver investment casting, the overall aim of still ongoing work is the further development of the simulation tool for gold alloys. This paper is a status report on the advances obtained so far in understanding different thermal properties of some 18K gold casting alloys, and how these properties influence solidification and susceptibility to porosity. Furthermore, the impact of thermal properties of investment material, as well as the potential role of different types of simulation software, is briefly discussed. The potential of simulation tools assisting in prevention and control of investment casting defects is indicated.

Introduction

Based on the formerly published achievements, the further development of computer simulation of jewelry investment casting for gold alloys, among others, requires substantial work on the following research tasks:

- Determination and validation of material property data for a variety of gold alloys and investment materials
- Computer simulation using different commercially available simulation software packages
- Experimental verification of simulation results by lab casting trials
- Demonstration of relevance for application by defect case studies on industrial casting defects

These would demand large personal and financial resources within long-term collaborative research projects, which have not been available in recent times. Hence, work at FEM dedicated to this topic was mainly restricted to cooperative projects with students from cooperating universities. However, a part of the results reported was obtained within a six-month collaborative research project funded by the regional consortium Arezzo Innovatione, Italy. Within the framework of that project, FEM started a cooperation with the research group from Politecnico de Torino, Campus Alessandria (CESAL), who were already working on casting simulation.[2] As a consequence, the work of FEM focused on the analysis of the solidification step, while the work of CESAL focused on the filling step (Figure 1), and corresponding results are reported in a separate paper by

Fischer-Bühner

Marco Actis Grande in these *Proceedings*.[4] The splitting up of these similarly important and complementary aspects has been judged useful for two main reasons:

- different experimental approaches have to be followed (data acquisition rates)
- different types of simulation software, probably with particular strengths, can be used.

1st step: mold filling / metal flow

CESAL:
- **Flow-3D – software**
- **Experimental data acquisition rate 1000/s**

2nd step: cooling / solidification

FEM:
- **MAGMASOFT® – software**
- **POLIGON – software**
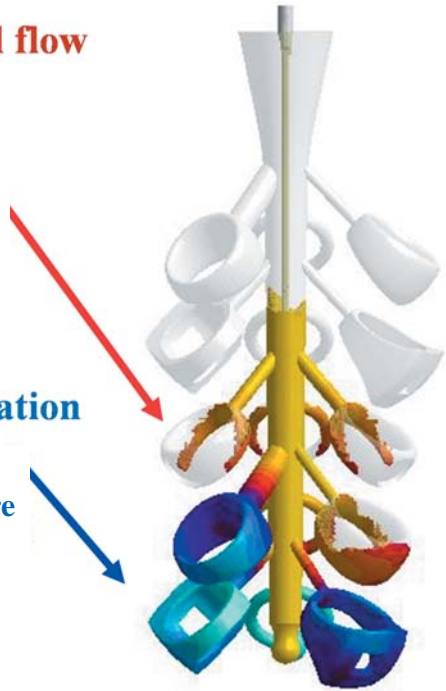- **Experimental data acquisition rate 50/s**

Figure 1 *The complementary nature of work at CESAL and FEM*

Working with Different Casting Simulation Software

Several widely recognized casting simulation software packages exist. Among others, they include MAGMASOFT®, ProCAST and FLOW-3D. To be more precise, the latter is in fact a general-purpose, fluid-flow modeling software that is not restricted to metal casting, which probably makes it particularly powerful for studying complex mold-filling scenarios.

In addition, many other casting simulation software packages do exist that are probably more focused either on specific industrial applications, or activities in their home countries. Among these is POLIGON, a Russian-made software we have been working with in addition to MAGMASOFT® in the recent months.

Advances in the Prevention of Investment Casting Defects . . .

It is far beyond the scope or objectives of our work to validate potential strengths and weaknesses of the different software packages. Some criteria of importance can be listed as follows:

- Software or license costs
- Calculation time
- General accuracy of results
- Suitability for solidification and/or filling phenomena
- Ease of use
- Demands on memory
- CAD environment included or not
- Enmeshment tool included or not
- Accuracy of geometrical details that can be realized
- Finite Element vs. Finite Difference concept

The last aspect is of great importance and has an impact on many of the other items on the list. Very simplified, it comes back to the point of whether the geometries are subdivided into rectangular elements (Finite Difference Modeling), or irregular shaped elements (Finite Element Modeling).

In cases where the simulation software does not include a CAD and Enmeshment tool (which applies to POLIGON), it is crucial to integrate powerful CAD into the workflow, as well as enmeshment software that can import/export geometry data in different data formats.

Figure 2 shows an example for a Finite Element Mesh of a research test tree and flask geometry generated with HyperMesh®, a renowned and specialized enmeshment software. Note the high spatial resolution of the Finite Element Mesh in regions where it is definitely required (pattern, feed-sprue and its direct environment in the mold), whereas a lower spatial resolution can be tolerated in the main sprue and especially in large areas of the mold.
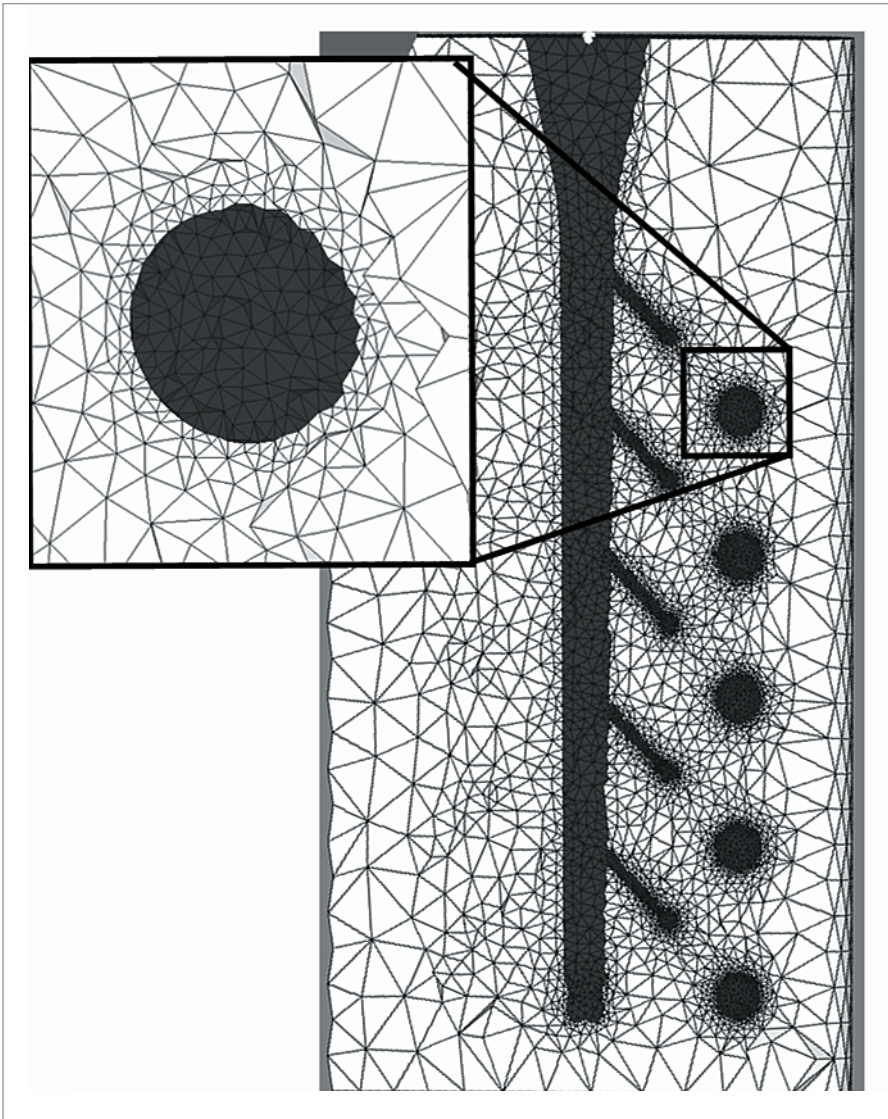
Fischer-Bühner

Figure 2 Two-dimensional mid-section of an example for
a Finite Element Mesh generated with HyperMesh®

Experimental

Three near-standard 18K gold alloys were selected as shown in Table 1 (all silicon-free). The temperature-dependent physical and thermal materials property data required for computer simulation were determined using NETZSCH thermoanalytical equipment (thermal diffusivity, thermal expansion, melting range, specific heat, etc.).

Advances in the Prevention of Investment Casting Defects . . .

Table 1 Composition of alloys (in weight °/oo) selected for the project

		Cu	Ag	Zn	Ni	add.
18K yellow	Legor A182N	91	157			2
	Standard 2N	90	160			
18K red	Legor OR134	233	11	5		1
	Standard 5N	200	50			
18K Ni white	Legor WH80B4	146		34	70	1
	Standard	145		35	70	

Experimental castings and corresponding simulations were carried out using standard casting process variables for the respective alloys, with

- T^{cast} : $\Delta T = 75–100°C$ (~130–180°F) above T^{liq}
- T^{flask} = 500°C (932°F)
- ~0.5 kg metal weight per tree
- pressure-assisted bottom-pouring vacuum casting (Indutherm VC 500)
- gypsum-bonded investment (SRS Classic for yellow/red gold; SRS Silk and R&R Ultravest for white gold).

The results were analyzed especially in terms of susceptibility to shrinkage porosity. This involved comparison of measured and simulated cooling curves for particular positions of test pattern, as well as comparison of simulated porosity levels with microscopic observations on metallographic cross-sections of as-cast samples.

In order to obtain consistent and reproducible experimental casting results with minimum gas porosity levels (which would interfere with shrinkage porosity phenomena in complex ways), special attention was given to optimizing melting and casting parameters, as well as investing and burnout parameters.

Thermal Properties of Alloys

Table 2 lists some thermal properties of the 18K gold alloys together with data for pure Au, Ag and sterling silver.

The 18K red alloy has the narrowest melting range of the three 18K alloys, but even the melting range of the 18K yellow alloy is still much narrower when compared to sterling silver. The data for the melting ranges are approximate values, since significant undercooling effects, which depend on cooling rates, may occur in real castings.

The heat of solidification (also called latent heat) varies only slightly for the three alloys, with the highest and lowest values for 18K yellow and 18K Ni white, respectively. All are near to the value known for pure gold, and are considerably below those for pure silver and sterling silver. This seemingly large difference between Au and Ag alloys levels off, however, as already pointed out earlier,[5] if the heat of solidification is computed per volume unit rather than per weight unit, yielding almost similar values around 1 kJ/cm³ for both classes of alloys.

Fischer-Bühner

	Melting range T^{sol}-T^{liq} , °C (°F)	Heat of solidification J/g	Thermal diffusivity at ~T^{liq} , mm²/s
18K yellow	900–930 (1652–1706)	75	25
18K red	890–900 (1634–1652)	66	25
18K Ni white	910–940 (1670–1724)	70	11
Fine Au	1064 (1947)	64	95*
Fine Ag	962 (1764)	107	130*
930 Ag	780–900 (1436–1652)	106	70

Data for thermal conductivities are not reported in Table 2. The thermal conductivity is defined as follows:

$$\lambda = \rho * c_p * a$$

with λ = thermal conductivity, ρ = density, c_p = specific heat capacity and finally, a = thermal diffusivity.

All these data are temperature-dependent and difficult to measure precisely. The accuracy of data obtained so far for density and specific heat capacity (of solid and especially molten material) would not allow for a meaningful discussion and, therefore, data are not reported here yet.

What can be reported and emphasized right now is that large differences in thermal conductivities exist between the 18K alloys. These are mainly related to large differences in thermal diffusivities as indicated in Table 2. 18K red and yellow gold have a similar thermal diffusivity at liquidus temperature, which is about a factor of 2.3 higher than for 18K Ni white. The thermal diffusivity of sterling silver is higher than for 18K yellow and red gold, however, namely by a factor of nearly 3 at liquidus temperature. The thermal diffusivities of all alloys are significantly lower than for the pure metals.

The computer simulation results shown in the following were obtained using the best available material data sets obtained so far. The results will have to be updated in the future, however, as soon as the accuracy of the materials data is improved.

COOLING CURVES IN EXPERIMENT AND SIMULATION

The tree set-up used is shown in Figure 3. The test pattern studied is a ring with a sphere of ~10mm diameter, with a feed-sprue of 3mm diameter, positioned either directly on the sphere, or at the opposite ring shank position. In addition, another test ring pattern (eccentric flat ring with two different feed-sprue positions) was added—an analysis of the corresponding results has not yet been completed, however.

Five patterns were each positioned along the main sprue (Neutec/USA® NeuSprue 7-inch) and cooling curves were analyzed for pattern in positions nearest to the main sprue tip and base respectively. Corresponding measured differences for pattern in the tip and base positions were less pronounced than reported earlier for sterling silver casting trials and will not be discussed here.

Figure 3 Left: as-cast 18K red gold tree after devesting;
right: wax tree with set of thermocouples

Figures 4 to 6 compare simulated and experimental cooling curves for the three 18K gold alloys. The simulation results shown were obtained with the POLIGON software, but are consistent with corresponding simulation results obtained with MAGMASOFT®.

The general characteristics of the experimental cooling curves, in terms of solidification and cooling kinetics for the different positions along the test pattern, are well reproduced by the simulation, despite the still non-optimum materials property data base. For the moment, more satisfying agreement between experimental and simulated behavior has been obtained for 18K red and white gold if compared to 18K yellow gold. It should be noted, however, that a considerable scatter in experimental data is commonly observed and the reasons for this will be discussed later.
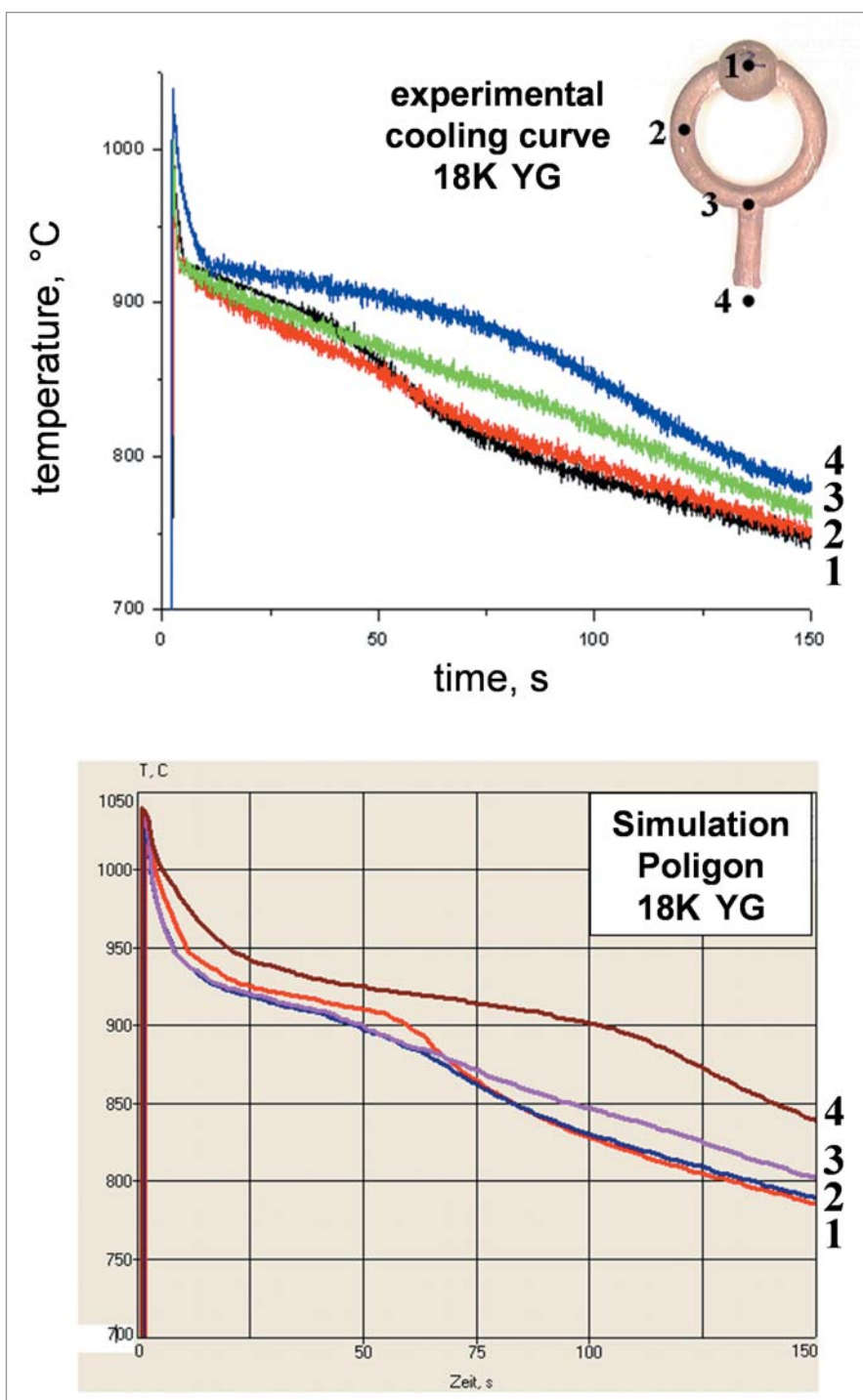
Fischer-Bühner

Figure 4 Comparison of measured and simulated cooling curve for 18K yellow gold
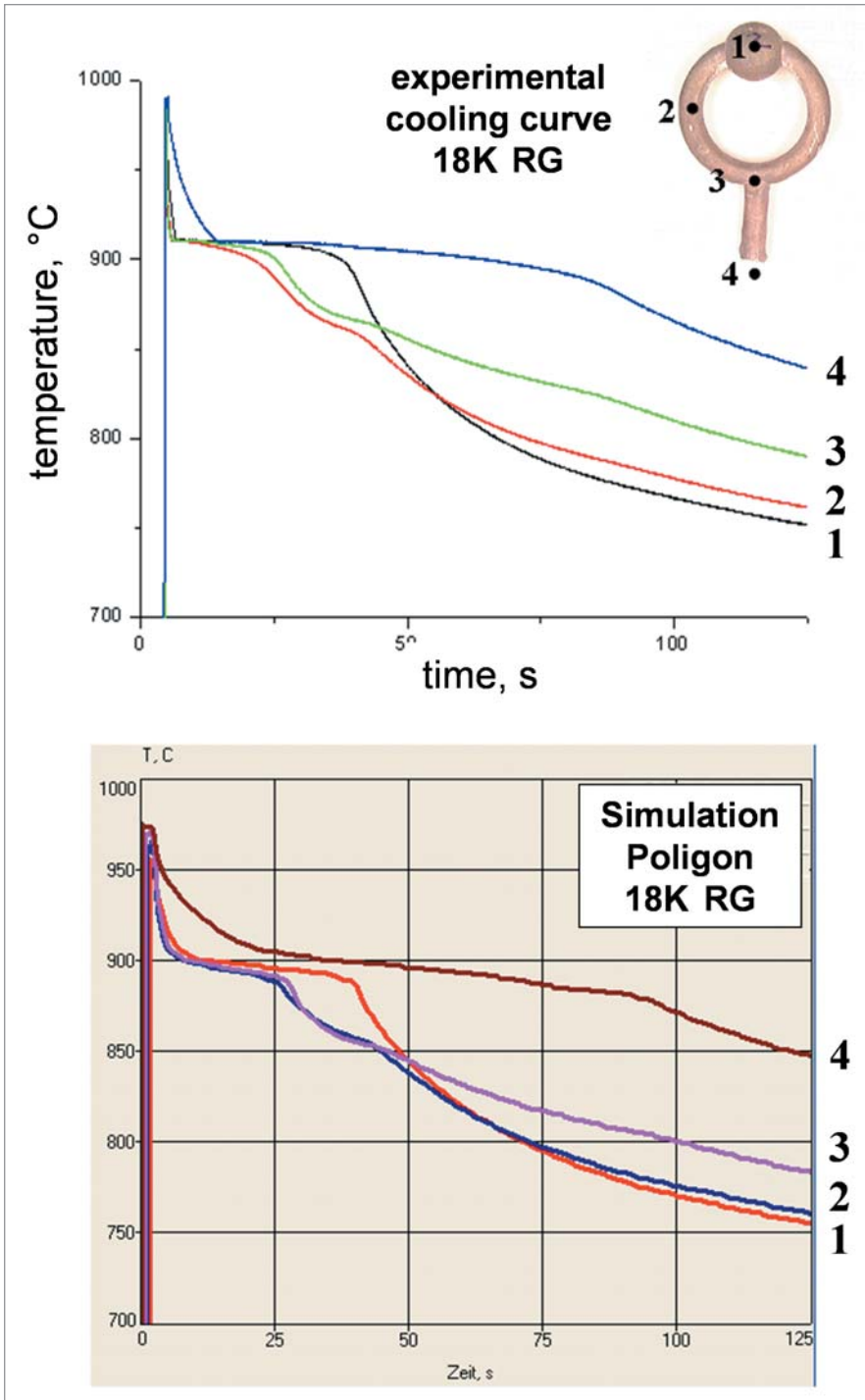
Fischer-Bühner

Figure 5 Comparison of measured and simulated cooling curve for 18K red gold

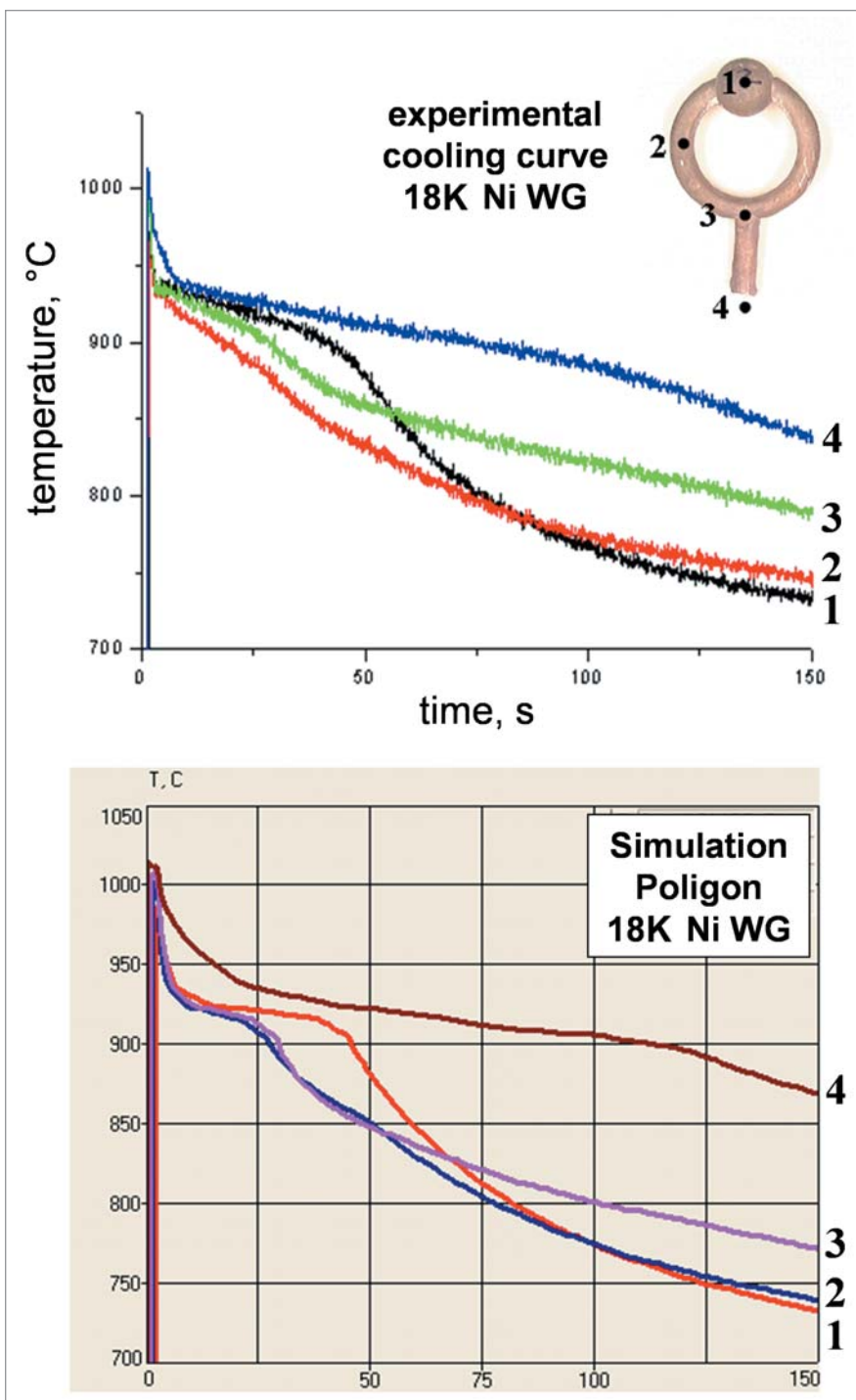*Figure 6* Comparison of measured and simulated cooling curve for 18K Ni white gold

Advances in the Prevention of Investment Casting Defects . . .

Shrinkage Porosity in Experiment and Simulation

Metallographic cross-sectional investigations were carried out on samples taken from the middle position on the main sprue. Figures 7 to 11 show the porosity levels as revealed on mid-plane sections for the three 18K alloys.

For 18K yellow the lowest porosity levels overall are observed with some micropores that accumulate in the sphere if the feed-sprue is in opposite position (Figure 7). For the same pattern, with identical feed-sprue position, heavy shrinkage porosity is observed for both 18K red and 18K Ni white gold (Figures 8 and 10), whereas samples from the same tree are virtually porosity-free if the feed-sprue is connected directly to the sphere (Figures 9 and 11).

The shrinkage porosity level observed in 18K Ni white is probably higher than in 18K red. This is difficult to assess, however, since in 18K Ni white the porosity has a pronounced interdendritic appearance and is located in the junction area of ring shank and sphere (Figure 10). In contrast, in 18K red, the porosity accumulates in the center of the sphere and forms macroscopic cavities (Figure 8).

Fischer-Bühner
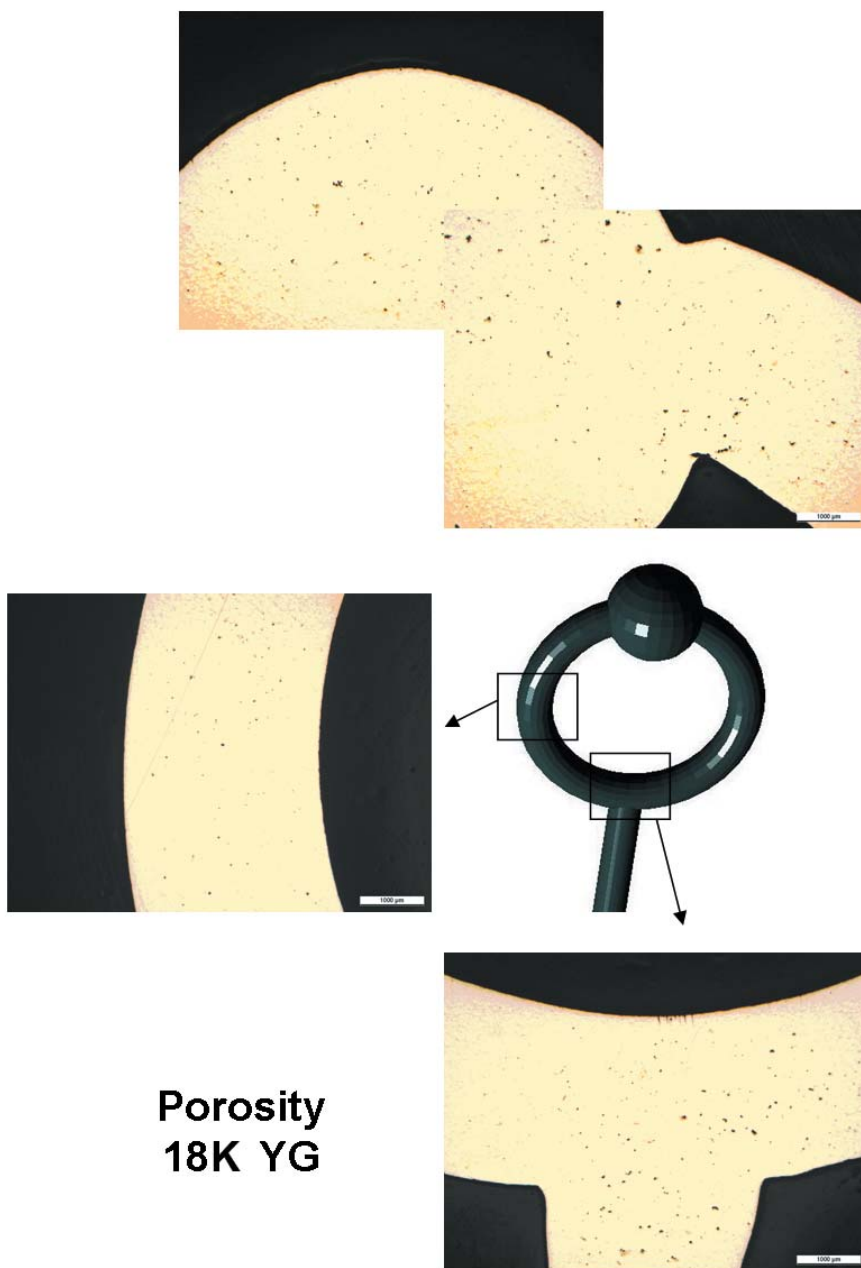
Porosity
18K YG

Figure 7 Metallographic investigation of porosity in 18K yellow gold.
The feed-sprue is positioned on the ring shank opposite to sphere.
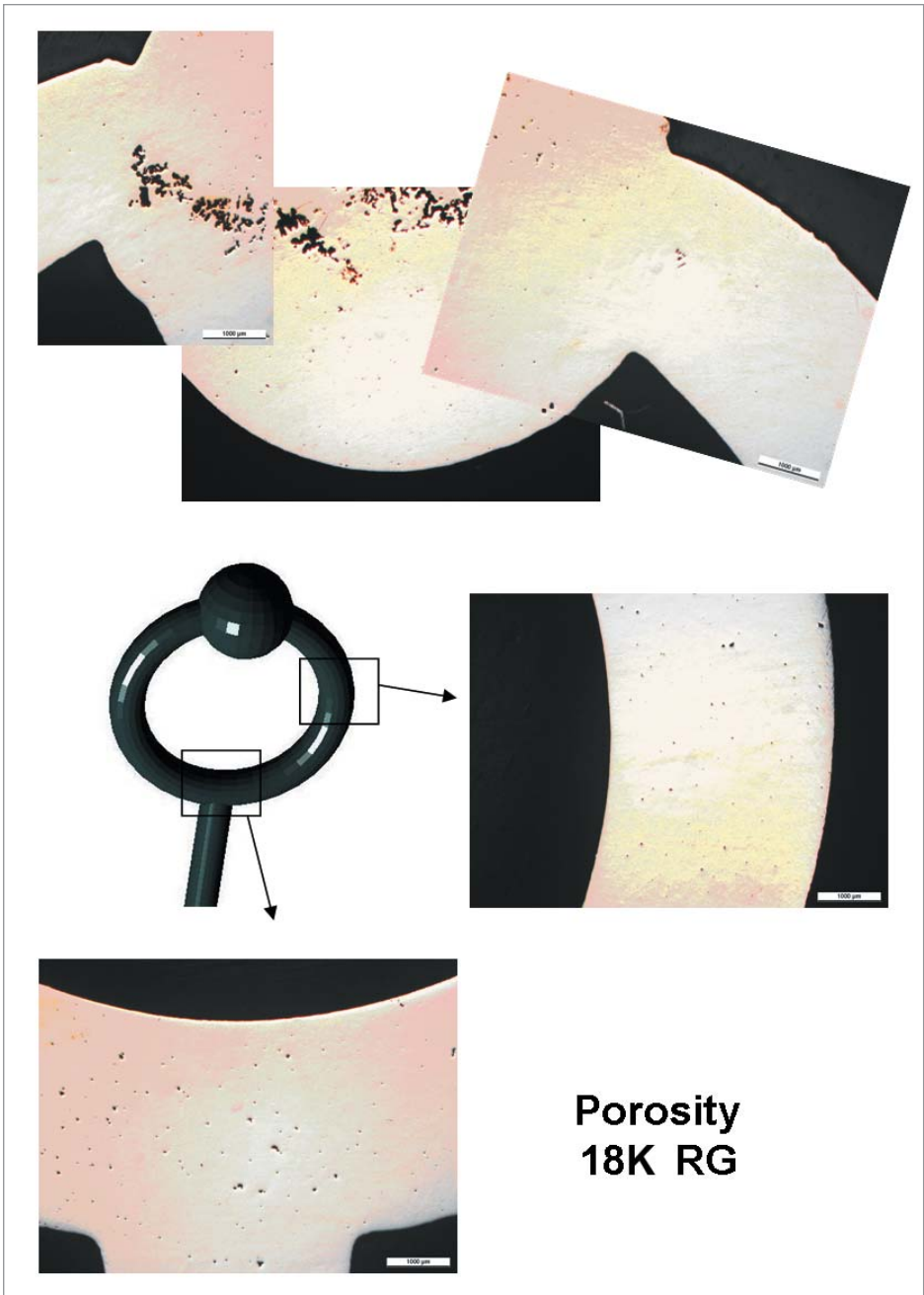
Figure 8 *Metallographic investigation of porosity in 18K red gold. The feed-sprue is positioned on the ring shank opposite to sphere.*
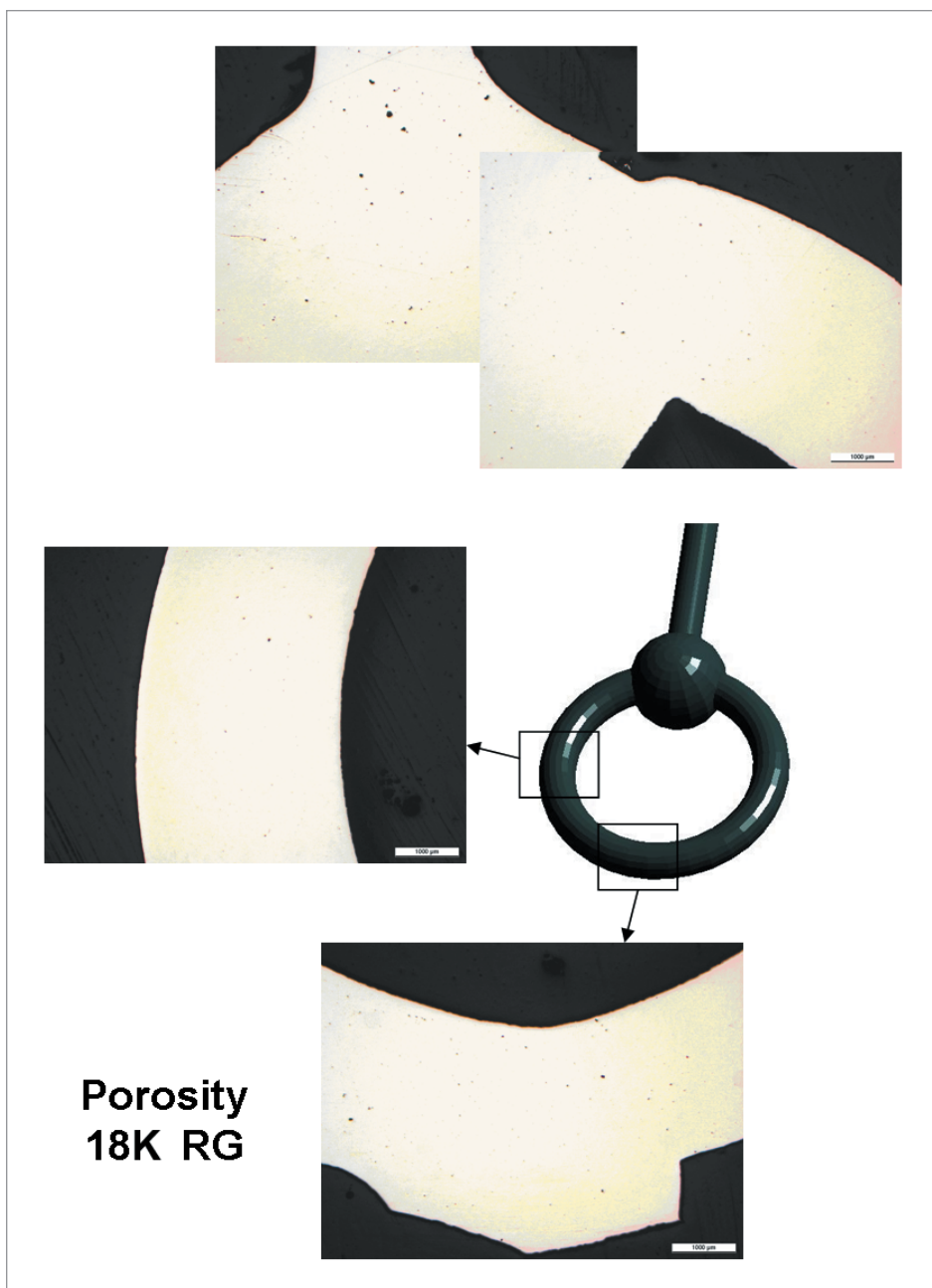
Porosity
18K RG

Figure 9 Metallographic investigation of porosity in 18K red gold.
The feed-sprue is connected directly to the sphere.

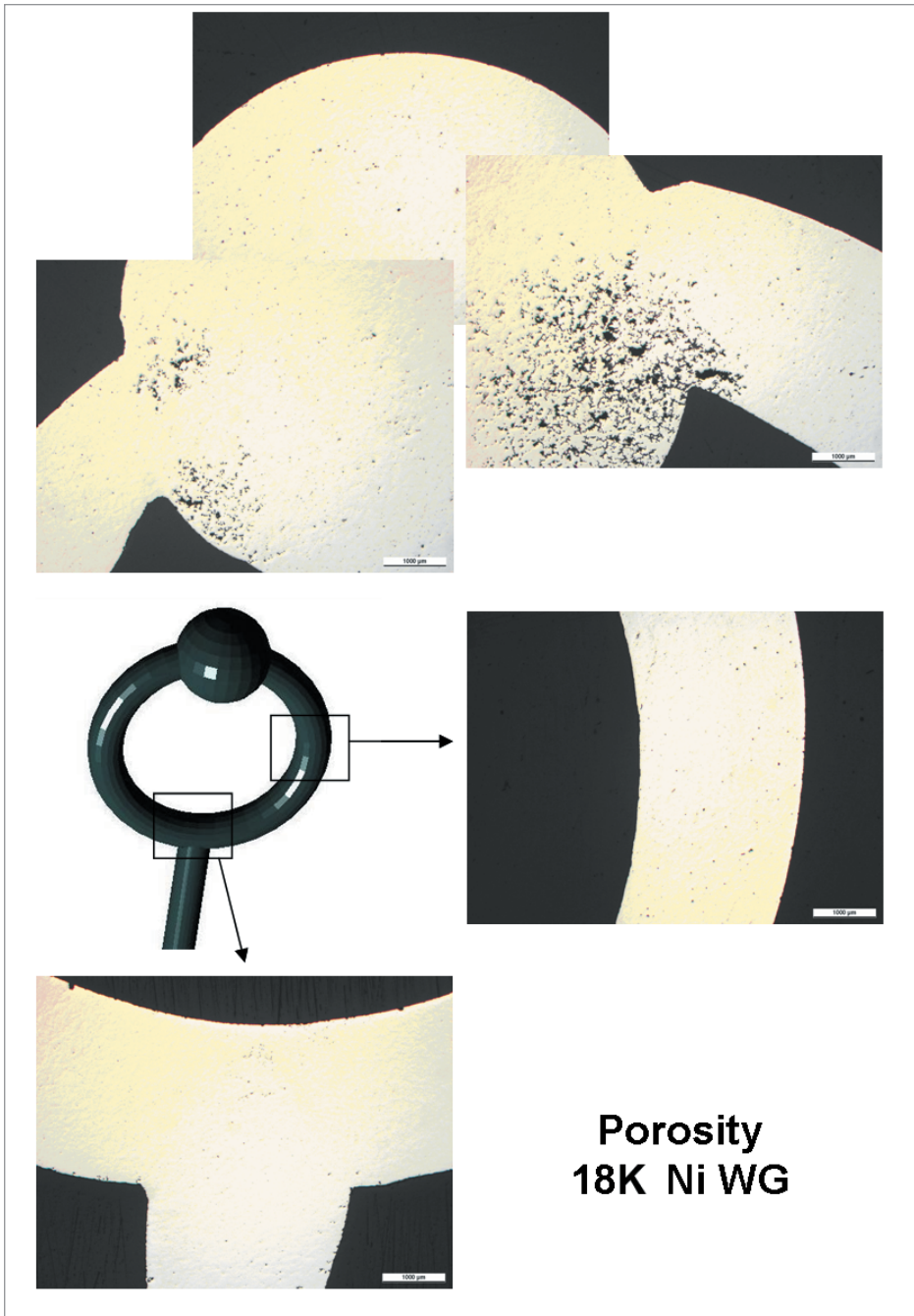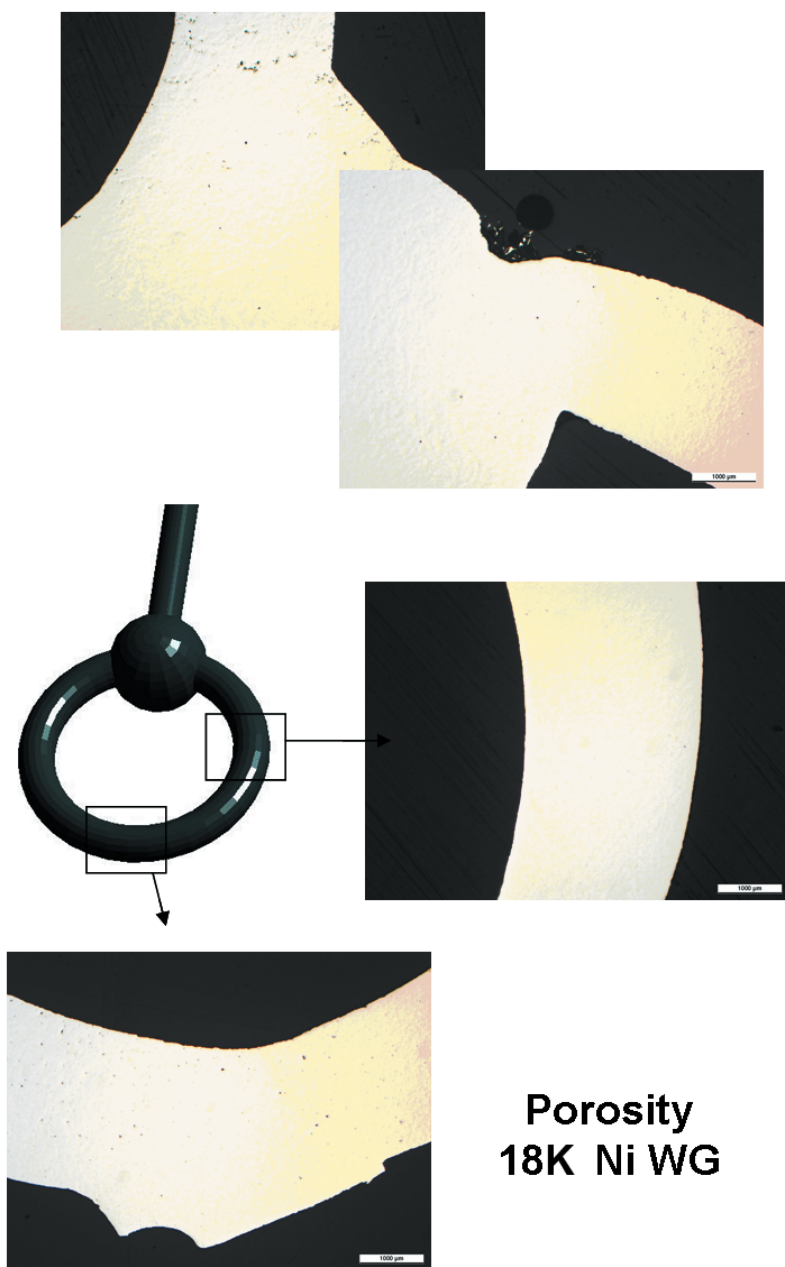*Advances in the Prevention of Investment Casting Defects . . .*

Fischer-Bühner

Figure 10 *Metallographic investigation of porosity in 18K Ni white gold. The feed-sprue is positioned on the ring shank opposite to the sphere.*

Figure 11 *Metallographic investigation of porosity in 18K Ni white gold. The feed-sprue is connected directly to the sphere.*

Some relevant trends in shrinkage porosity evolution are well reproduced by the simulations shown in Figures 12 and 13. The white sections represent areas with zero shrinkage porosity, whereas grey-shaded areas visualize regions where the simulation predicts shrinkage porosity. The scales that are used differ from alloy to alloy, but these scales are less telling if not shown in color, hence the areas with high porosity are also marked by arrows in Figure 13.

The overview for 18K yellow in the Figure 12 example shows that very little variation in shrinkage porosity is predicted for these patterns along the main sprue.

Figure 13 compares the simulated porosity levels for a single test pattern. In accordance with the experimental results, high shrinkage porosity levels are predicted for the sphere in 18K Ni white and 18K red gold, whereas a low shrinkage porosity level (<1%) is predicted for 18K yellow gold. For this particular pattern, and the casting parameters applied, the highest susceptibility to shrinkage porosity is predicted for 18K Ni white gold.

The exact locations, as well as the local amount ("100%") where shrinkage pores form in the sphere region, are not predicted accurately by these simulations. Similar to the results obtained with POLIGON, MAGMASOFT® also predicts an accumulation of porosity in the upper half of the spheres. Without going into details, it seems that consideration of processes happening on the microstructural level, probably only in a phenomenological way in the simulation, are required to address this problem.
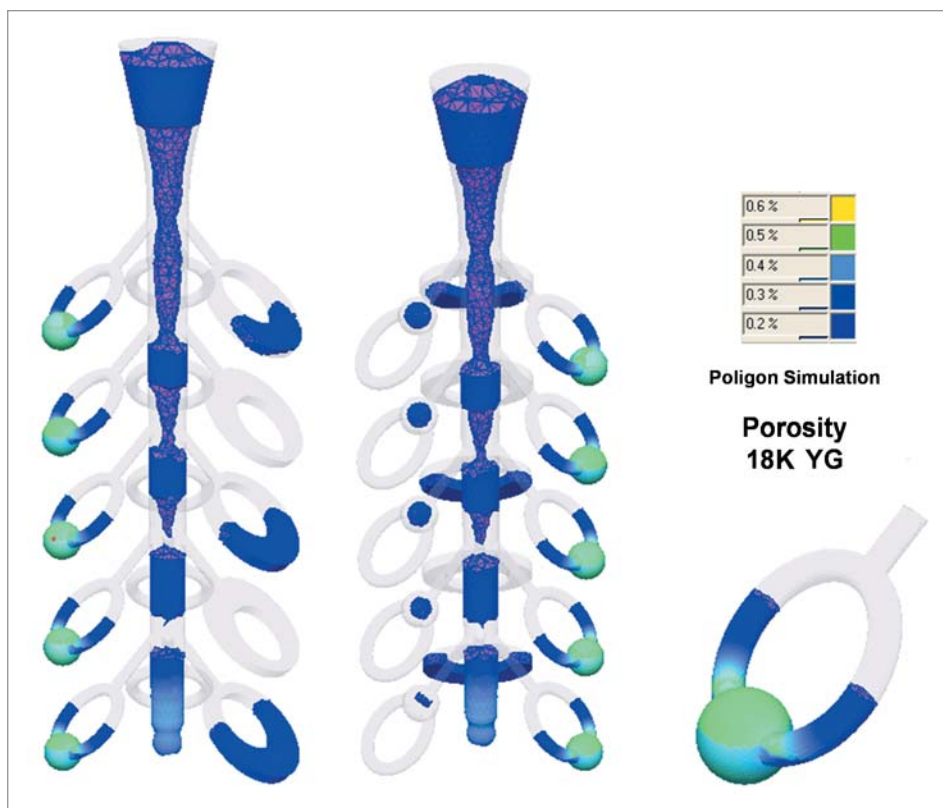
Fischer-Bühner

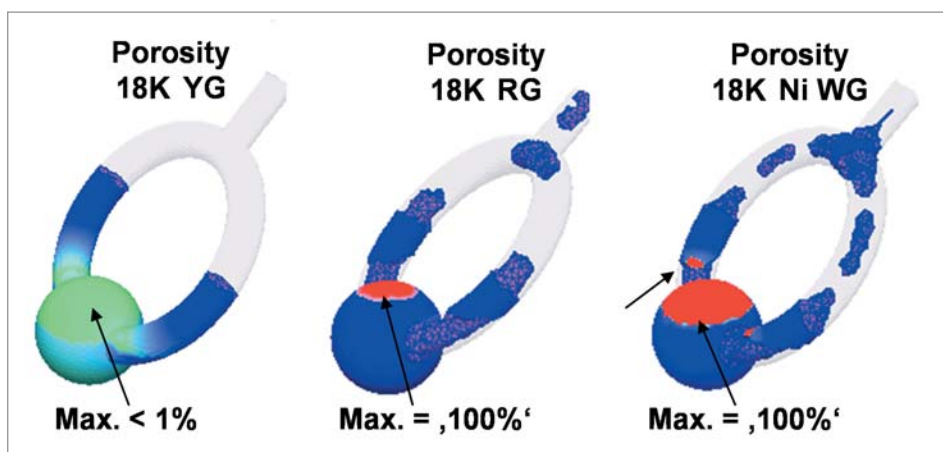*Figure 12* Overview on simulated shrinkage porosity in 18K yellow gold

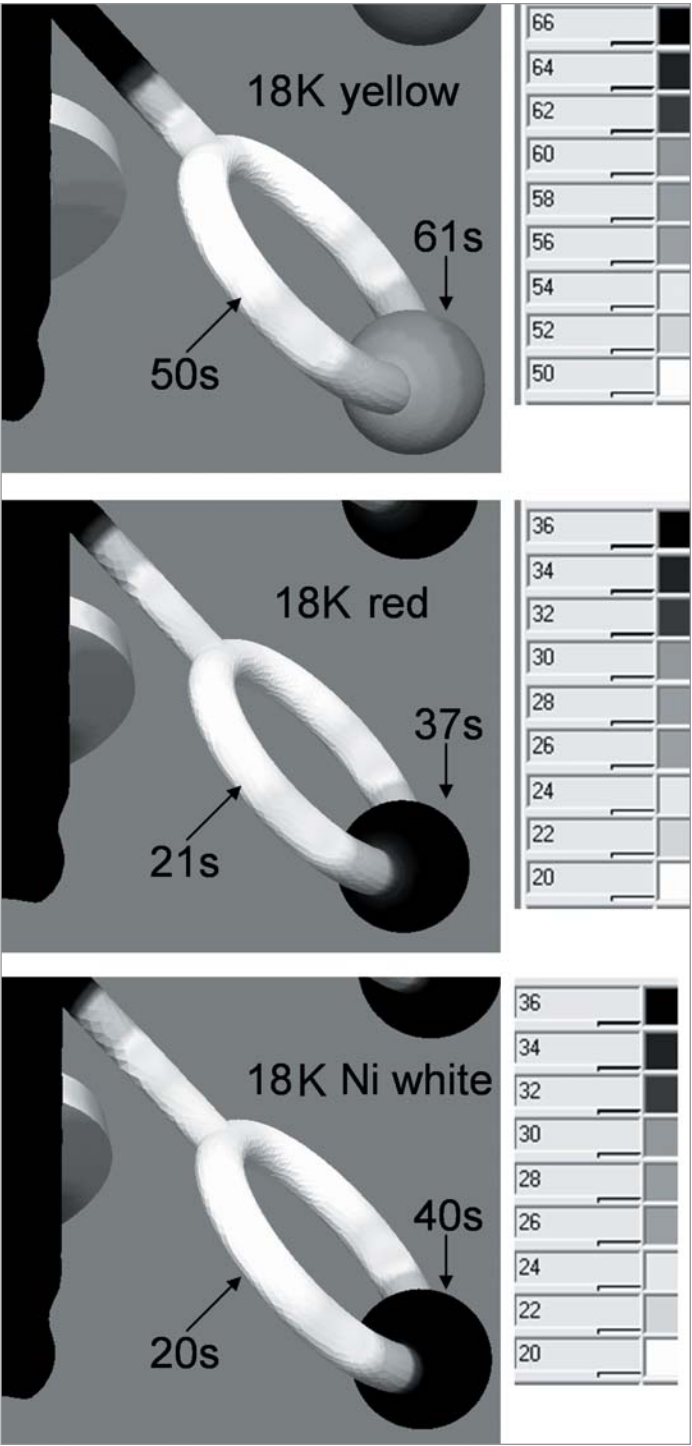*Figure 13* Comparison of simulated shrinkage porosity in 18K gold alloys

Figure 14 *Comparison of simulated solidification time profiles for 18K gold alloys*

Preliminary Correlation of Thermal Properties with Susceptibility to Shrinkage Porosity

From our former work on sterling silver,[1] we need to keep in mind the importance of the tremendously low thermal conductivity of the investment material if compared to all casting alloys, independent of their chemical composition. This leads to a quick and strong heat-up of the mold material layers in direct contact with the melt during, and especially after, filling. Unless filigree items are considered, where solidification takes place already during filling,[4] this leads to an insulating effect of the mold material during the solidification step. In sterling silver, which has a comparably high thermal diffusivity, as well as a wide melting range of $\Delta T = \sim 120°C$ (216°F), the heat stored in the main sprue heavily controls the solidification of the pattern by the heat flow through the feed-sprue. This leads to comparably long solidification times in sterling silver (~90s in the sphere), and comparably little shrinkage porosity for the identical particular pattern and the casting conditions studied in this paper.

Taking this into consideration, the analysis of the simulated solidification time profiles shown in Figure 14, together with the data reported in Table 2, may allow us to draw some further conclusions about the 18K alloys studied in the present work.

Let us first compare 18K Ni white gold with yellow gold: They have a comparable heat of solidification and a similar melting range of $\Delta T = \sim 30°C$ (54°F) in the same temperature range. Due to the significantly lower thermal diffusivity of the Ni white gold, the heat stored in the main sprue has much less influence on the solidification of the pattern when compared to the yellow gold. First, this results in much faster solidification kinetics of the Ni white gold. Second, this results in much more pronounced temperature gradients along the feed-sprue, ring shank and pattern during the cooling process, eventually leading to large differences in solidification time of ring shank (local minimum) and sphere (local maximum) in the Ni white gold (Figure 14). This yields much higher shrinkage porosity in the sphere for the same pattern cast in 18K Ni white gold when compared to 18K yellow gold.

The thermal diffusivities of 18K red gold and yellow gold are comparable, but for the 18K red gold the heat of solidification is somewhat smaller and especially the melting range is much more narrow with $\Delta T = \sim 10°C$ (18°F), obviously contributing to the observed shorter solidification times. Despite similar thermal diffusivity, this does not allow the heat in the main sprue to control the solidification in the same way as in 18K yellow gold, eventually leading to a solidification time profile and shrinkage porosity level that is comparable to the situation obtained in 18K Ni white gold.

Obviously, we need to have the complete overview on all relevant thermal properties including, especially, the specific heat capacity and the density (percentage of shrinkage during solidification) to come to conclusions of general validity. Furthermore, this demands studies on different patterns and casting conditions.

Fischer-Bühner

Advances in the Prevention of Investment Casting Defects . . .

Advances in Prevention of Investment Castings Defects Assisted by Computer Simulation

Coming back to the promise provided by the title of this paper, we agree that further improvements of the materials property data base and verification by experimental and industrial castings are required to satisfy it. However, the level of agreement already obtained between experimental and simulated casting results may allow us to use the simulation tool in a pragmatic way, not only for sterling silver, but also for the range of 18K alloys studied so far.

Figure 15 shows how this tool can be used to identify improved, or even optimized, feed-sprue geometries and positions for two different jewelry patterns and the three 18K alloys, taking into account their thermal properties in the simulation. It shows the shrinkage porosity as predicted by MAGMASOFT® simulations for the three 18K gold alloys for some samples near to the sprue tip. Again, the white sections represent areas with zero shrinkage porosity, whereas grey-shaded areas visualize regions where the simulation predicts shrinkage porosity.
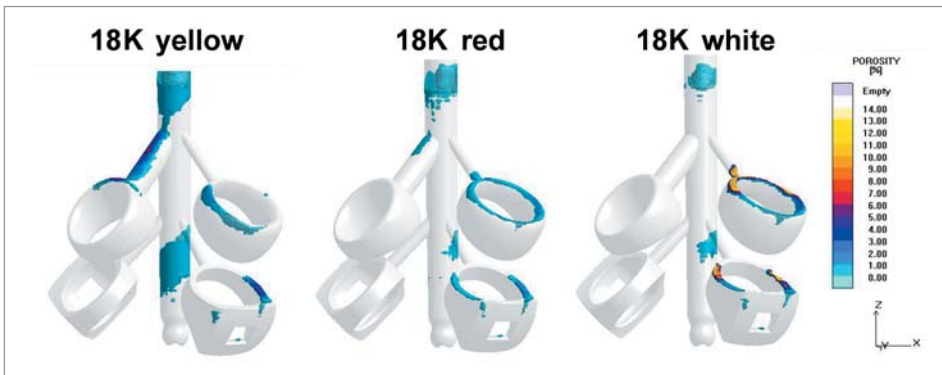

Figure 15 *Simulated shrinkage porosity levels for the three 18K gold alloys for comparable casting conditions and a flask temperature of 500°C (932°F)*

Obviously, for the pattern in the right row, the same feed-sprue diameter and position leads to the most pronounced shrinkage porosity in the 18K Ni white gold alloy when compared to the yellow and red gold alloy. Repositioning the feed-sprue, and increasing its diameter (pattern in the left row), leads to zero shrinkage porosity for the white and red gold alloy, whereas, in the case of the upper ring, the thick feed-sprue obviously is not an optimum choice for the yellow gold alloy.

These results strictly correlate with the thermal properties of the different alloys as discussed in the former chapter. They indicate that different optimum solutions in feed-sprue design exist depending on alloy composition, whereas, a "one-size-fits-all" policy is still more common in industrial production processes. Improved consideration of these aspects assisted by computer simulation should be helpful in reducing defect rates caused by shrinkage porosity phenomena.

Fischer-Bühner

Impact of Thermal Properties of Investment Material

During our experimental casting trials in recent years, where cooling curves were recorded on a routine basis, a considerable scatter in experimental data (among others, solidification times) was obtained even if casting parameters were kept nominally constant.

While it is reasonable to assume that the thermal properties of casting alloys do not change significantly with small variations in alloy composition, several process parameters may be responsible for this behavior, including accuracy of casting temperature and flask temperature, investing and burnout process, as well as type and actual batch of investment material.

In accordance with the experience of many industrial casters, the control of process parameters that are set via the casting equipment, like casting temperature and overpressure, are usually not considered a problem. It is well known that in a standard burnout oven (without forced air circulation) and depending on its construction, the temperature distribution can be problematic, leading to non-uniform temperatures within single flasks, or from one flask to the other. This explains some of the scatter we observed in measured solidification times and shrinkage porosity levels which may critically depend on flask temperature. For certain, a burnout oven with even temperature distribution, forced air circulation, or a rotary burnout oven are essential in order to obtain consistent results, not only in research, but, of course, also in production.

We have also been using investment materials from different suppliers, as well as different batches of investment from the same supplier. Without having profound enough property data from our ongoing research, the impression is that thermal properties vary to an extent that may significantly influence the solidification process. As revealed earlier by the simulations, the low thermal conductivity of the mold material is a very significant factor in the solidification process. Sensitivity analysis using computer simulation indicates that even small variations in thermal conductivity can have a profound influence. More research is required to study these issues.

Summary and Conclusion

The main achievements of the work so far can be summarized as follows:

- The measurement of material property data reveals large differences in thermal properties for differently colored 18K gold alloys, especially with regard to thermal diffusivities.

- A satisfying agreement between experiment and simulation of the casting and solidification process is now obtained for some standard 18K gold alloys, in addition to sterling silver.

- The different thermal properties of alloys lead to largely different susceptibility to shrinkage porosity and demand for alloy-specific feed-sprue design in order to obtain optimum casting quality.

- Computer simulation is an increasingly valuable tool that assists in identifying optimum feed-sprue systems and process parameters aimed at the minimization of investment casting defects.

Advances in the Prevention of Investment Casting Defects . . .

Fischer-Bühner

Enormous further research efforts are required, however, to widen the potential application of casting simulation tools to the large variety of casting alloys. It needs to be stressed that close cooperation with industrial partners during such work is mandatory in order to verify the relevance of the work for industrial casting processes and problem-solving in daily production.

References

1. Jörg Fischer-Bühner, "Computer Simulation of Jewelry Investment Casting: What Can We Expect?," in *The Santa Fe Symposium on Jewelry Manufacturing Technology 2006,* ed. Eddie Bell (Albuquerque: Met-Chem Research, 2006): 193; and in *Proceedings of 3rd International Conference on Jewelry Production Technology* (JTF, Vicenza/Italy), 2006: 240.

2. Marco Actis Grande, et al., "Numerical Simulation of the Investment Casting Process: Experimental Verification," in *Proceedings of the 2nd International conference on Jewelry Production Technology*, (JTF Vicenza/Italy), 2005: 93.

3. Jörg Fischer-Bühner, "Improvement of Sterling Silver Investment Casting", in *The Santa Fe Symposium on Jewelry Manufacturing Technology 2006,* ed. Eddie Bell (Albuquerque: Met-Chem Research, 2006): 217; and in *Proceedings of 3rd International Conference on Jewelry Production Technology* (JTF, Vicenza/Italy), 2006: 122.

4. Marco Actis Grande, "Computer Simulation of the Investment Casting Process: Widening of the Filling Step," in *The Santa Fe Symposium on Jewelry Manufacturing Technology 2007,* ed. Eddie Bell (Albuquerque: Met-Chem Research, 2007): 1.

5. Dieter Ott, "Properties of Melt and Thermal Processes During Solidification in Jewelry Casting," in *The Santa Fe Symposium on Jewelry Manufacturing Technology 1999,* ed. Dave Schneller (Albuquerque: Met-Chem Research, 1999): 487.

Fischer-Bühner